




Comprehensive analysis of keloid vasculature by tissue clearing and 3D imaging

Long Nguyen MD¹ | Teruyuki Dohi MD, PhD¹  | Haruko Watanabe-Takano PhD² | Shigetomo Fukuhara PhD²  | Rei Ogawa MD, PhD, FACS¹ 

¹Department of Plastic, Reconstructive and Regenerative Surgery, Nippon Medical School, Tokyo, Japan

²Department of Molecular Pathophysiology, Institute of Advanced Medical Sciences, Nippon Medical School, Tokyo, Japan

Correspondence

Teruyuki Dohi, Department of Plastic, Reconstructive and Aesthetic Surgery, Nippon Medical School, 1-1-5 Sendagi, Bunkyo-ku, Tokyo 113-8603, Japan.
Email: dohiprs@gmail.com

Haruko Watanabe-Takano, Department of Molecular Pathophysiology, Institute of Advanced Medical Sciences, Nippon Medical School, 1-1-5 Sendagi, Bunkyo-ku, Tokyo 113-8603, Japan.
Email: t-haruko@nms.ac.jp

Shigetomo Fukuhara, Department of Molecular Pathophysiology, Institute of Advanced Medical Sciences, Nippon Medical School, 1-1-5 Sendagi, Bunkyo-ku, Tokyo 113-8603, Japan.
Email: s-fukuhara@nms.ac.jp

Abstract

Keloids are a complex type of scar tissue formed by exaggerated wound healing, characterised by the overgrowth of thick fibrous tissue beyond the original wound boundary. While the crucial relationship between keloid formation and the vascular system has been highlighted, conflicting findings have been reported regarding the characterisation of keloid vasculature. Here, we successfully characterised the detailed three-dimensional (3D) structure of vasculature in keloid tissues using tissue clearing methods combined with 3D imaging. First, we compared two optical tissue clearing methods, the clear, unobstructed brain imaging cocktails and computational analysis and immunolabelling-enabled 3D imaging of solvent-cleared organ protocols, and found the latter to provide greater transparency of keloid scars. We then conducted a detailed 3D vascular analysis using light sheet and confocal fluorescence microscopy. In normal skin, capillary loops and the superficial vascular plexus were located in the papillary layer and at the boundary between the papillary and reticular layers, respectively. However, the density of these vessels was higher in keloid scars than in normal skin. The reticular layer of normal skin exhibited fewer blood vessels. In contrast, keloid scars exhibited significantly thickened dermal reticular layers, with the upper reticular layer showing significantly greater vascularisation. The lower reticular layer of keloid scars also exhibited vertically aligned blood vessels, although their density was lower than in the upper reticular layer. These results indicate that excessive vascularisation is predominantly induced in the papillary and upper reticular layers of keloid scars, which might contribute to keloid pathogenesis. The technique described here has the potential to serve as a crucial template for future pathological analyses of abnormal scars.

Abbreviations: 2D, two-dimensional; 3D, three-dimensional; CUBIC, clear, unobstructed brain imaging cocktails and computational analysis; DBE, dibenzyl ether; DCM, dichloromethane; DMSO, dimethyl sulfoxide; HKC, hyalinised keloïdal collagen; iDISCO+, immunolabelling-enabled 3D imaging of solvent-cleared organs; RT, room temperature; VEGF, vascular endothelial growth factor. Teruyuki Dohi and Haruko Watanabe-Takano co-second authors.

This is an open access article under the terms of the [Creative Commons Attribution-NonCommercial-NoDerivs](https://creativecommons.org/licenses/by-nc-nd/4.0/) License, which permits use and distribution in any medium, provided the original work is properly cited, the use is non-commercial and no modifications or adaptations are made.

© 2025 The Author(s). *Wound Repair and Regeneration* published by Wiley Periodicals LLC on behalf of The Wound Healing Society.

KEYWORDS

CUBIC, iDISCO+, keloid, pathologic scars, tissue clearing

1 | INTRODUCTION

A keloid is a complex type of scar tissue formed by exaggerated wound healing, characterised by the growth of thick fibrous tissue beyond the original wound boundary.¹ Unlike normal scars, keloids exhibit persistent inflammation and continuous growth, failing to regress naturally over time.^{2,3} This fibroproliferative disorder of the skin poses a considerable challenge for medical treatment due to its persistent nature and high recurrence rate.⁴

Recent research has highlighted the crucial relationship between keloid formation and the vascular system. Angiogenesis is thought to be actively induced in keloid tissues, generating abnormal blood vessels.⁵ Reportedly, vascular endothelial growth factor (VEGF), a potent inducer of angiogenesis, is consistently upregulated in keloid tissues compared to normal skin.^{6,7} Furthermore, recent studies have provided evidence of vascular dysfunction and hypoxia within keloid tissues.^{8,9} Reports indicate low regional oxygen saturation and vascular congestion in keloid cores, indicating hypoxic conditions associated with impaired blood flow and vascular occlusion. Fibroblasts isolated from patients with keloids also exhibit elevated expression of VEGF and transforming growth factor- β .¹⁰ These findings highlight the importance of endothelial cells and pericytes in the fibrotic process of keloids. Indeed, increasing evidence suggests that endothelial dysfunction and pericyte activation contribute to the fibrotic process.^{11,12} Furthermore, studies have shown that hyalinised keloidal collagen (HKC), a characteristic feature of keloids, is closely associated with vascular structures, suggesting that blood vessels might play a role in the formation and progression of HKC.^{13,14} Recent single-cell RNA sequencing analyses have also identified distinct fibrovascular interactions and endothelial cell enrichment in keloid tissues, highlighting the dynamic interplay between endothelial cells and fibroblasts in keloid pathogenesis.¹⁵

Although the role of vascular changes in keloid development has been acknowledged, there is ongoing discussion about the precise nature and importance of these alterations. Considerable controversy exists regarding the vascular characteristics of keloids.^{16–19} While some studies have reported high vascular density in keloids,^{16,18} others suggest that keloids exhibit poor vascularisation.^{17,19} This discrepancy can be partly attributed to the limitations of conventional histochemistry, which relies on two-dimensional (2D) slicing and might not fully capture the complex three-dimensional (3D) structure of keloid vasculature.²⁰

To address these limitations, advanced imaging techniques, such as tissue clearing combined with 3D imaging, have emerged as promising approaches. These techniques, including clear, unobstructed brain imaging cocktails and computational analysis (CUBIC) and immunolabelling-enabled 3D imaging of solvent-cleared organs (iDISCO+), enable the reconstruction of 3D structural images with exceptionally high resolution, while maintaining tissue integrity.^{21–25}

Indeed, Tan et al. have applied tissue clearing methods combined with 3D imaging to visualise cutaneous nerves in human skin.^{26,27}

The present study aimed to perform a detailed characterisation of the 3D structure of keloid tissue vasculature by leveraging these advanced tissue clearing methods combined with 3D imaging. We successfully cleared keloid tissues using the iDISCO+ tissue clearing method and captured the 3D structure of keloid vasculature. By comparing keloid vasculature with that of normal skin, we demonstrated that excessive blood vessel formation occurs in the papillary and upper reticular layers of keloid scars, which might contribute to the pathogenesis of keloids.

2 | MATERIALS AND METHODS

2.1 | Human skin and keloids

Twenty-five patients clinically diagnosed with keloid scars and planning to undergo surgical treatment were included in this study. A total of 18 keloid samples and 14 normal skin samples were obtained from various regions of each patient's body, such as the head, face, ears, chest, arms, abdomen, and pubic area (Table 1). To compare the vascular structures in normal and keloid tissues, normal skin tissues from the face, chest, and pubic area were taken from areas adjacent to the keloid scars in the same patients, as shown in Table 1. The protocols for obtaining human tissue samples for tissue clearing were approved by the Ethics Committee of Nippon Medical School Hospital, Tokyo, Japan. Written informed consent was obtained from all participants.

2.2 | Antibodies and nuclear staining

The anti-human CD31 antibody (FLEX Monoclonal Mouse Anti-Human CD31, Endothelial Cell, Clone JC70A, Dako Omnis, Agilent Technologies, Santa Clara, CA, USA) was used as the primary antibody. Goat anti-mouse IgG Alexa Fluor 647 (Jackson ImmunoResearch Labs, West Grove, PA, USA; dilution 1:400) was used to visualise the primary antibody. Nuclei were stained with DAPI (Thermo Fisher Scientific, Waltham, MA, USA; final concentration 20 μ M).

2.3 | Sample preparation

Two types of samples were evaluated: keloids and normal skin. Normal skin samples were obtained at least 0.3 cm away from the scar edge. Immediately after dissection, the samples were fixed in 4% paraformaldehyde (PFA) in phosphate-buffered saline (PBS) for 1 day at 4°C. After fixation, the tissue samples were washed with PBS at 4°C. Then, the samples were either cut into approximately 1-mm-thick



TABLE 1 Sample collection information of study participants, including ID, age, gender, and area for keloid and normal skin samples.

Keloid				Skin			
Patients	Age	Gender	Area	Patients	Age	Gender	Area
K1	23	F	Ear	S1	36	M	Chest
K2	27	F	Ear	S2	51	F	Face
K3	50	F	Ear	S3	77	M	Face
K4	30	M	Chest	S4	43	F	Arm
K5	35	F	Ear	S5	73	F	Face
K6	34	F	Ear	S6	30	M	Chest
K7	63	M	Back	S7	30	F	Back
K8	43	F	Abdomen	KS1	34	M	Chest
K9	26	M	Face	KS2	27	F	Face
K10	23	F	Ear	KS3	39	M	Pubic
K11	29	M	Abdomen	KS4	35	M	Chest
KS1	34	M	Chest	KS5	28	M	Chest
KS2	27	F	Face	KS6	58	F	Chest
KS3	39	M	Pubic	KS7	29	F	Face
KS4	35	M	Chest				
KS5	28	M	Chest				
KS6	58	F	Chest				
KS7	29	F	Face				

slices to obtain 3D images of the vasculature or dissected to prepare 5-mm-thick tissue blocks for observation using a light sheet microscope. To assess the efficiency of tissue clearing using the CUBIC and iDISCO+ protocols, the keloid samples were cut into 1-mm-thick and 5-mm-thick slices.

2.4 | Tissue clearing using the CUBIC protocol followed by immunostaining

2.4.1 | Tissue clearing

The keloid tissue samples were processed for optimal clearing and imaging according to the CUBIC protocol.^{23,28,29} Initially, the tissue samples were immersed in a 50% CUBIC-1 solution [25% N,N,N',N'-Tetrakis ((2-hydroxypropyl)ethylenediamine) (Tokyo Chemical Industry, TCI, Tokyo, Japan), 25% Urea (Nacalai Tesque, Kyoto, Japan), and 15% polyethylene glycol mono-p-isooctylphenyl ether (TritonX-100) (Wako Pure Chemical Industries, Osaka, Japan)] diluted with H₂O at 37°C for 6 h. Then, the samples were soaked in a 100% CUBIC-1 solution at 37°C for 14 days, during which time the solution was changed every 48 h. Thereafter, the samples were carefully rinsed three times with PBS.

2.4.2 | Immunostaining

For immunostaining, the tissue samples were placed in staining buffer [PBS containing 5% normal donkey serum (Jackson ImmunoResearch, West Grove, PA, USA) and 0.25% Triton X-100 (Sigma-Aldrich,

St. Louis, MO, USA)] overnight at 37°C. Then, the samples were stained with anti-CD31 antibody in staining buffer at 37°C for 4 days. After washing with PBS three times for 1 h each with gentle shaking at room temperature (RT), the keloid tissues were incubated with a secondary antibody diluted in staining buffer at 37°C for 4 days. After incubation, the samples were washed three times with PBS for 1 day at RT to remove any excess antibody. Finally, the samples were soaked in CUBIC-2 solution [50% Sucrose (Nacalai Tesque, Kyoto, Japan), 25% Urea (Nacalai Tesque, Kyoto, Japan), 10% 2,2',2''-nitrilotriethanol (Wako Pure Chemical Industries, Osaka, Japan), and 1% Triton X-100 (Sigma-Aldrich, St. Louis, MO, USA)] at RT on the last day to complete the clearing process.

2.5 | Tissue clearing using the iDISCO+ protocol followed by immunostaining

2.5.1 | Methanol pretreatment

The keloid tissues and normal skin samples were processed according to the iDISCO+ protocol.^{24,30} First, the samples were dehydrated in methanol (MeOH) diluted with H₂O at 4°C at the following concentrations, each for 1 h: 20%, 40%, 60%, 80%, and 100% MeOH, and transferred to a mixture of 33% MeOH and 66% dichloromethane (DCM) (Sigma-Aldrich, St. Louis, MO, USA) overnight at RT. Then, the samples were immersed in 100% MeOH twice for 1 h each and soaked in 5% H₂O₂/MeOH overnight at 4°C. After incubation, the samples were rehydrated using a reverse MeOH series (80%, 60%, 40%, and 20% MeOH in H₂O) and stored in PBS at RT.

2.5.2 | Immunostaining

The tissue samples were incubated in PBS containing 0.2% Triton X-100 (PTx.2) twice for 1 h at RT. They were then permeabilised in PTx.2 containing 20% dimethyl sulfoxide (DMSO) (Nacalai Tesque, Kyoto, Japan) and 2.3% glycine (Nacalai Tesque, Kyoto, Japan) overnight at 37°C and blocked with PTx.2 containing 6% normal donkey serum and 10% DMSO (blocking solution) for 2 days at 37°C. Subsequently, the samples were stained with anti-CD31 antibody in the ready-to-use solution with gentle shaking at 37°C for 7 days. After incubation, the samples were washed with PTwH [PBS containing 10 µg/mL heparin (Nacalai Tesque, Kyoto, Japan) and 0.2% Tween-20 (Sigma-Aldrich, St. Louis, MO, USA)] at RT, with the solution being changed 4 to 5 times until the following day. Finally, the samples were incubated with the secondary antibody in PTwH for 7 days at 37°C with gentle shaking, followed by washing with PTwH at RT, with the solution being changed 4 to 5 times until the following day.

2.5.3 | Tissue clearing

The immunostained keloid tissues were dehydrated as described in section 2.5.1. The samples were then incubated in a mixture of 33% MeOH and 66% DCM for 3 h, followed by two washes with 100% DCM for 15 min each at RT. Finally, the samples were incubated in dibenzyl ether (DBE) (Tokyo Chemical Industry, TCI, Tokyo, Japan) at RT until they became transparent.

2.6 | Imaging

2.6.1 | Confocal microscopy

Tile scan fluorescent imaging of skin sections mounted on glass slides submerged with DBE was performed using a FLUOVIEW FV3000 confocal microscope (Olympus, Tokyo, Japan) equipped with a 10× dry objective lens (UPlanApo, Olympus) operated with FLUOVIEW FV31S-SW software (Olympus). Individual tiles were acquired as Z-stacks consisting of approximately 100 slices at 4 µm intervals, and large images were obtained by digitally stitching each tile with a 10% overlap between neighbouring tiles (3 × 3 fields for keloid skin and 3 × 2 fields for normal skin). Composite images were processed using Imaris software version 10.0.1 (Imaris Bitplane, Zurich, Switzerland), and maximum intensity projections were then generated.

2.6.2 | Light sheet fluorescence microscopy

After cleaning, the large keloid biopsy was placed in a Quartz glass tube (Q-204, AzLab Quartz Cell, Axel Global, Tokyo, Japan) filled with DBE (Tokyo Chemical Industry, TCI, Tokyo, Japan) and photographed using desktop-equipped SPIM for cleared specimens, descSPIM³¹ with a combined 2× objective lens (0.1 NA). Time-lapse images were

obtained with an exposure time of 100 ms and a stage velocity of 100 µm. The relative velocity of the two actuators was estimated following the method previously described by Otomo et al.³¹ The captured Z-stack images were processed using ImageJ software version 1.5.4 (National Institutes of Health, Bethesda, MD, USA), and 3D image reconstruction was performed using Imaris version 10.0.1 software (Oxford Instruments, Abingdon, UK) with a voxel size of $3.45 \times 3.45 \times 10 \mu\text{m}^3$.

2.7 | Quantitative analysis of imaging data

To quantitatively analyse vascular structures, six consecutive Z-plane images, corresponding to a 20-µm-thick section, were randomly extracted from the confocal images of vasculature in keloid and normal skin, obtained as described in section 2.6.1, and used to generate 2D projection images. For the analysis of vasculature in the papillary layer, regions of interest (ROIs) of $150 \mu\text{m} \times 150 \mu\text{m}$ were placed starting from the top surface of the papillary layer. For normal skin samples, additional ROIs of the same size ($150 \mu\text{m} \times 150 \mu\text{m}$) were placed 150 µm below those in the papillary layer to analyse the vascular structure in the reticular layer. For the analysis of vasculature in the reticular layers of keloid samples, an additional two ROIs, each separated by 150 µm, were placed 150 µm below those in the papillary layer and designated as 'Reticular-1' and 'Reticular-2', respectively, since the reticular layers in keloid tissue were significantly thicker than those in normal skin. These ROIs were positioned at depths of 300–650 µm and 650–1000 µm from the skin surface, respectively. For each area, a total of 60 independent, non-overlapping ROIs were selected from keloid and adjacent normal skin tissues from four patients, ensuring data representativeness.

The acquired images were then processed through steps, such as conversion to 8-bit, median filtering, binarisation, and skeletonisation. ImageJ software with Vascular Density and Analyse Skeleton plugins^{32,33} was used to quantify vascular density, average vascular diameter, and the number of branching points. Vascular density was quantified as the percentage of the CD31 fluorescence-positive pixels relative to total analysed pixels using 60 ROIs per region. The number of vessel branch points was quantified as the number per 1 µm of vessel length. Average vessel diameter was quantified by dividing the total vascular area by the total vascular length. ROIs that did not contain any CD31 fluorescence-positive pixels were excluded from the quantification of vessel branch points and average vessel diameter. These vascular characteristics, when analysed through 2D imaging, were considered significant for quantitatively measuring the structure of vessels.³⁴ This process was specifically conducted for the quantitative analysis of vascular structures in both normal skin and keloid tissue samples.

2.8 | Statistical analysis

GraphPad Prism software version 10.2.2 (GraphPad Software, San Diego, CA, USA) was employed for data analysis. Normality was

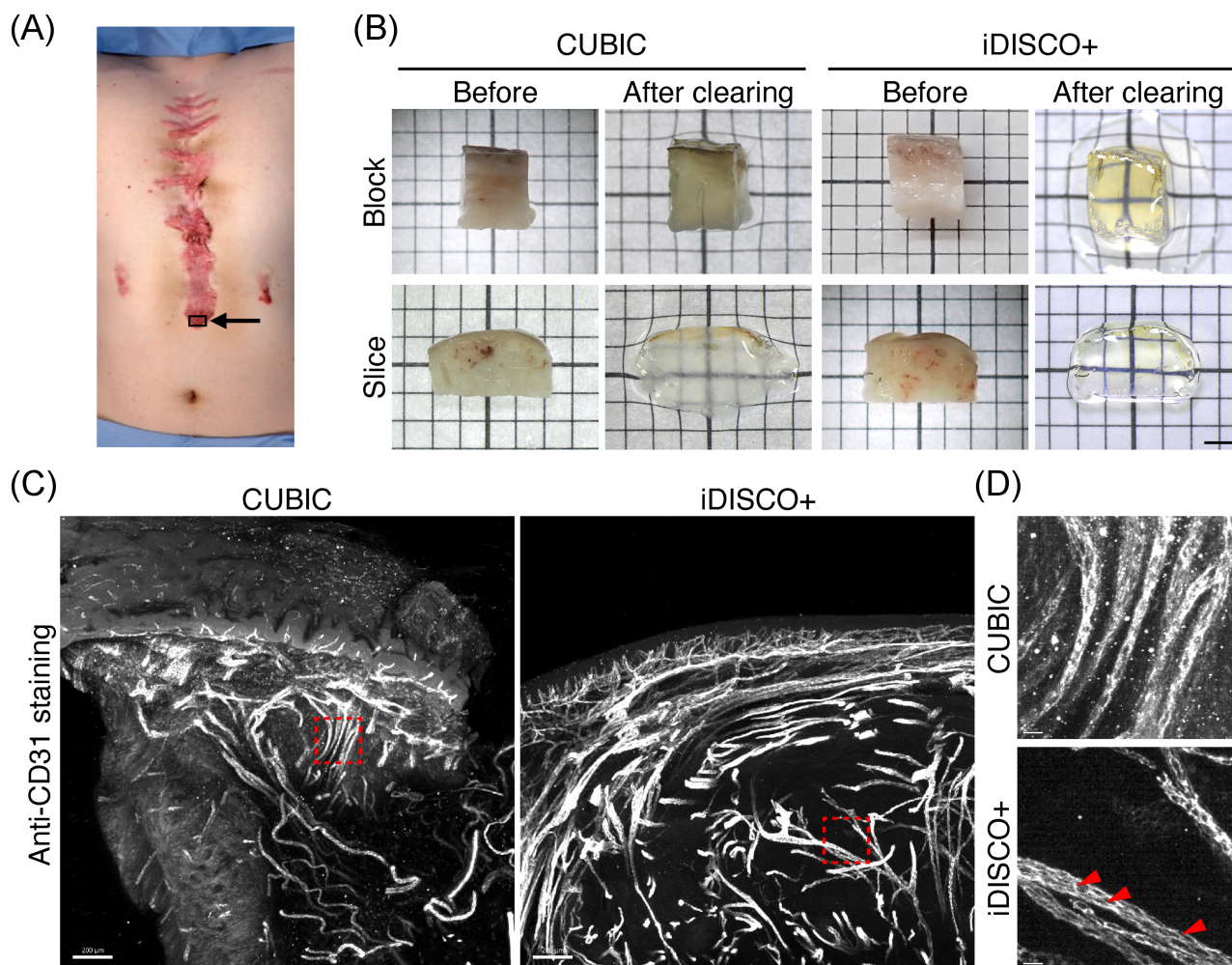


FIGURE 1 Comparison of CUBIC and iDISCO+ methods for clearing keloid tissues. (A) Keloid scar in the patient's abdominal region, with the black arrow indicating the site analysed. (B) Keloid scars before and after clearing using the CUBIC (left) and iDISCO+ (right) protocols. The upper and lower panels show block samples (5 mm thick) and sliced samples (1 mm thick), respectively, placed on graph paper. Each side of square on the graph paper represents 2 mm. (C) Confocal Z-projection images of anti-CD31 antibody-labelled blood vessels in 1 mm-thick keloid scars cleared using the CUBIC (left) and iDISCO+ (right) protocols. The images were generated by projecting a stacked series of approximately 100 slices, each acquired at 4 μ m intervals, covering a total thickness of 400 μ m. (D) Enlarged images of the boxed areas in (C). The arrowheads in the iDISCO+ image indicate a clearer signal of anti-CD31 antibody-labelled blood vessels compared to the CUBIC image. Scale bars: 200 μ m (C) and 20 μ m (D).

assessed graphically and supplemented by the Shapiro–Wilk test. Statistical tests were conducted based on vascular characteristics, such as vascular density, diameter, and the number of branching points. The Kruskal–Wallis test, followed by Dunn's post hoc test, was used for comparison of vascular structures in both papillary and reticular layers between normal skin and keloids.

3 | RESULTS

3.1 | Development of a tissue-clearing method for keloid scars using the iDISCO+ protocol

First, we compared two optical tissue clearing methods, the CUBIC and iDISCO+ protocols, to efficiently clear the keloid tissues. Keloid

tissues were excised from one of the patient's abdomen (Figure 1A). After fixation with 4% PFA, block (5-mm-thickness) and slice (1-mm-thickness) samples were cleared and immunostained using the CUBIC and iDISCO+ protocols, as described in section 2. The slice samples of keloid tissues became transparent with both clearing methods (Figure 1B). However, the transparency of the keloid tissues was higher when cleared using the iDISCO+ protocol compared to the CUBIC protocol (Figure 1B). Consistently, the keloid tissue block cleared using the iDISCO+ protocol also exhibited greater transparency compared to the one cleared using the CUBIC protocol. In addition, clearing keloid tissue using the iDISCO+ protocol resulted in clearer fluorescence signals of blood vessels stained with the anti-CD31 antibody compared to the CUBIC protocol (Figure 1C, D). Based on these results, we decided to use the iDISCO+ protocol to clear keloid tissues for subsequent analyses.

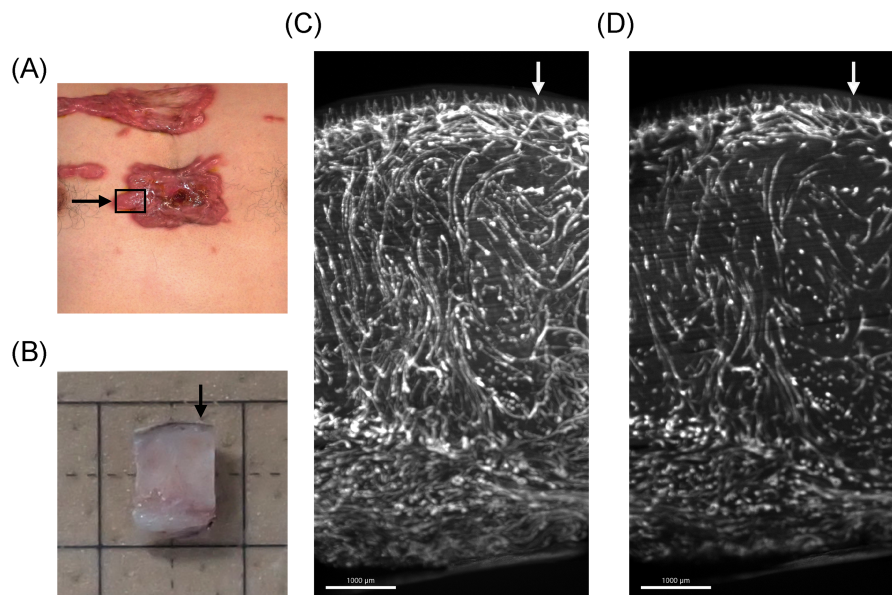


FIGURE 2 Visualisation of the entire vascular structure in keloid tissue using a light sheet fluorescence microscope. (A) Keloid scar in the patient's chest, with a block arrow indicating the analysed site. (B) Block tissue sample from a chest keloid (approximately 5 mm in width \times 7 mm in height \times 5 mm in thickness) used for 3D fluorescence imaging. Each side of square drawn by bold line on the graph paper represents 1 cm. (C, D) Z-projection of a 3D fluorescence image obtained from a 500- μ m-thick tissue section (C) and a single-slice image (D) showing the entire vascular structure of the keloid scar. The keloid scar, cleared using the iDISCO+ protocol, was immunostained with anti-CD31 antibody and imaged using a light sheet fluorescence microscope. Note that the superficial layers near the skin surface of the keloid scar exhibit a higher density of blood vessels, whereas the deeper regions have a relatively lower density, with most blood vessels being vertically aligned. Scale bars: 1 mm. In (B–D), arrows indicate the skin surface.

3.2 | Visualisation of the entire vascular structures in keloid scars using a light sheet fluorescence microscope

To comprehensively understand the entire vascular structures in keloids, the keloid tissue blocks excised from the patient's chest and abdominal skin were cleared using the iDISCO+ protocol and immunostained with anti-CD31 antibody (Figures 2A,S1). The vascular structures were then imaged using a light sheet fluorescence microscope. The 3D images revealed that vascular density was higher in the superficial layer of keloids than in the deeper regions. Consistently, the corresponding cross-sectional slice views confirmed that dense vascular networks were predominantly located in the upper dermal layers, including the papillary dermis and upper reticular dermis. On the other hand, the deeper regions had a relatively lower density of blood vessels, many of which were vertically aligned. These results suggest that angiogenesis might be more actively induced in the superficial layer of keloids compared to the deeper layer.

3.3 | Formation of excessive blood vessels in keloid scars

Next, we analysed the vascular structures in keloid scars and normal skin from various regions, such as the face, chest, back, pubic area, arm, ear, and abdomen (Figures 3,S2). To this end, we immunostained

cleared 1-mm-thick sections of keloid scars and normal skin with anti-CD31 antibody and imaged them using a confocal microscope. In normal skin, capillary loops were formed in the papillary layer of the dermis, while the superficial vascular plexus was situated at the boundary between the papillary and reticular layers. The reticular layer of normal skin exhibited fewer blood vessels but contained vertically aligned vessels that connected to the superficial vascular plexus at the boundary between the dermis and hypodermis.^{35,36} Keloid scars also contained capillary loops in the papillary layer of the dermis and a superficial vascular plexus at the boundary between the papillary and reticular layers. However, the density of these vessels was observed to be higher than in normal skin. In addition, the keloid scars exhibited significantly thickened dermal reticular layers compared to normal skin, as previously reported.³⁷ Importantly, these thickened reticular layers were occupied by a dense, vertically aligned vascular plexus. These findings indicate excessive blood vessel formation in keloid scars across various anatomical regions. However, a more comprehensive analysis is needed to elucidate site-specific vascular characteristics in keloid scars.

3.4 | Analysis of vascular abnormalities in keloid scars

To further clarify the abnormalities in vascular structures in keloids, we quantified the vascular density, number of vessel branch points



relative to the vessel length, and vessel diameter in the chest keloid scars and adjacent normal skin (Figure 4). Since 3D fluorescence images of keloid tissues obtained using a light sheet

fluorescence microscope showed greater vascularisation in the upper dermal layer compared to the deeper layer (Figure 2), we primarily focused on the upper dermal layer, including the papillary dermis and

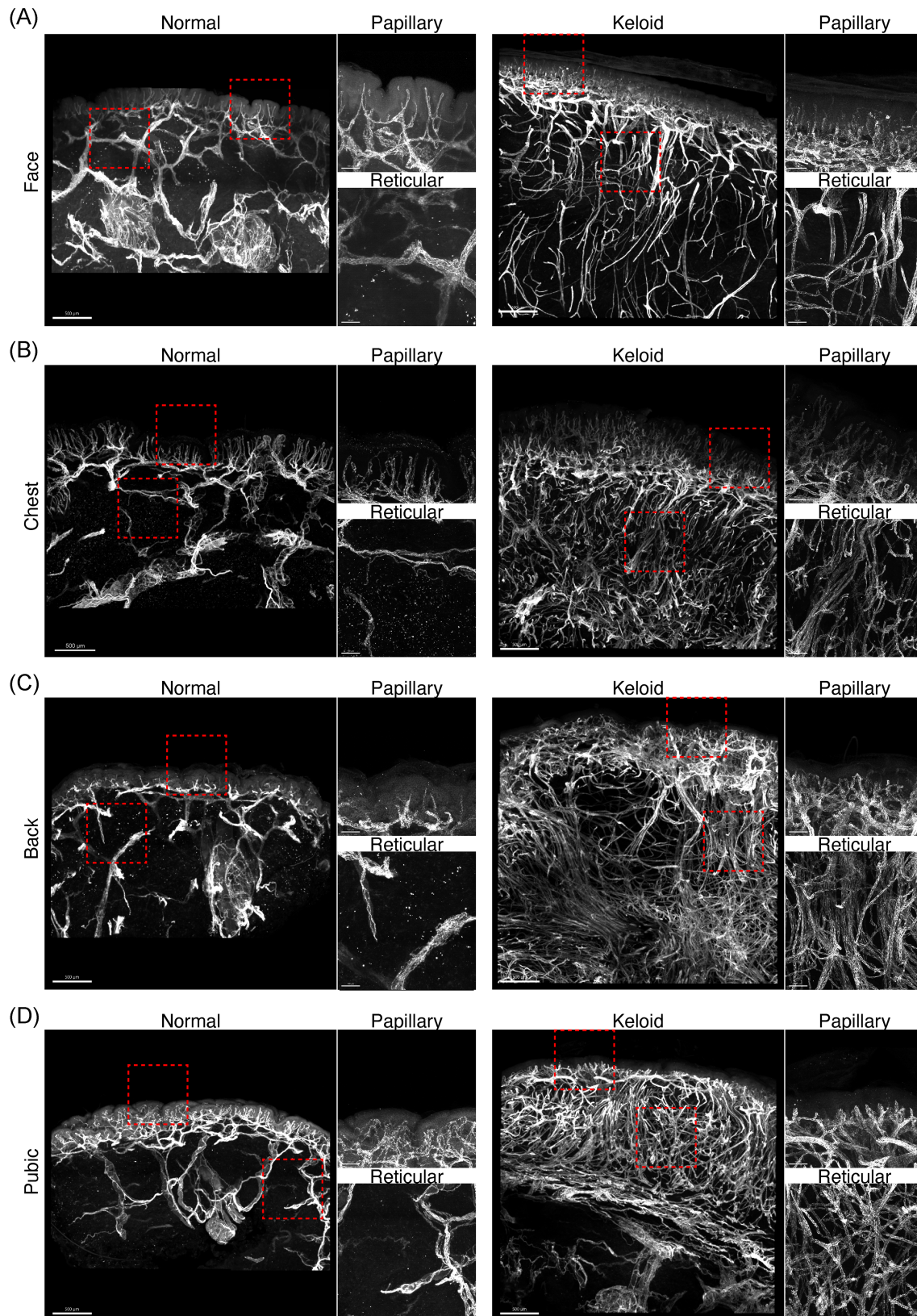


FIGURE 3 Legend on next page.

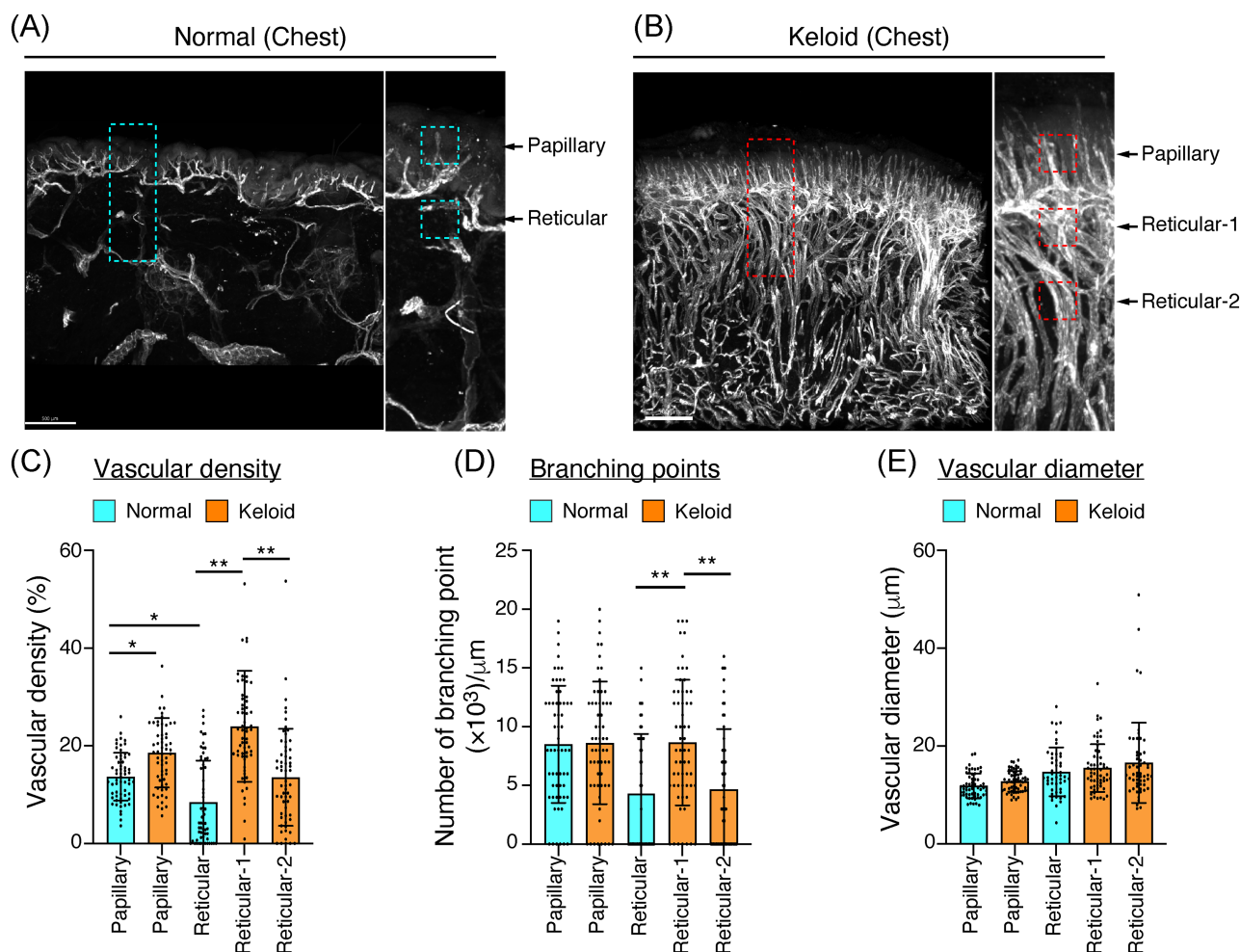


FIGURE 4 Quantitative analysis of vascular abnormalities in keloid scars. (A, B) Confocal Z-projection images of anti-CD31 antibody-labelled blood vessels in a keloid scar (B) and the adjacent normal skin (A) from the chest region. The images were generated by projecting a stacked series of approximately 100 slices, each acquired at 4 μm intervals, covering a total thickness of 400 μm. The boxed areas are enlarged on the right. Scale bars: 500 μm. (C–E) Quantification of the vascular density (C), number of vessel branch points relative to vessel length (D), and vessel diameter (E) in the papillary and reticular layers of the dermis, as shown in (A, B). For quantification, 2D projection images were generated from six consecutive Z-plane images, corresponding to a 20-μm-thick section, extracted from confocal images of vascular structures in keloid and the adjacent normal skin. These images were analysed as described in section 2.7. The boxed areas labelled ‘Papillary’ in the enlarged images in (A) and (B), corresponding to regions between 0 and 150 μm from the top of the papillary layer, were analysed as the papillary layer. The boxed area labelled ‘Reticular’ in the enlarged image of (A), corresponding to regions between 300 and 450 μm, was analysed as the reticular layer in normal skin. In contrast, two distinct regions labelled as ‘Reticular-1’ and ‘Reticular-2’ in the enlarged image of (B), corresponding to areas between 300 and 450 μm and 600 and 750 μm from the top of the papillary layer, respectively, were analysed as the reticular layers in the keloid scar. Data are presented as mean ± SD, with dots representing each individual value. (C) $n = 60$ ROIs for each group; (D) and (E), $n = 48, 55$ and 60 ROIs for the normal reticular layer, keloid reticular layer-1 (Reticular-1), and other groups, respectively. The Kruskal–Wallis test, followed by Dunn’s post hoc test, was used for statistical evaluation. * $p < 0.05$. ** $p < 0.01$.

FIGURE 3 Comparison of vascular structures in keloid scars and normal skin across various anatomical regions. (A–D) Confocal Z-projection images of anti-CD31 antibody-labelled blood vessels in normal skin (left) and keloid scars (right) from the face (A), chest (B), back (C), and pubic (D) regions. The images were generated by projecting a stacked series of approximately 100 slices, each acquired at 4 μm intervals, covering a total thickness of 400 μm. Normal skin tissues were collected from areas adjacent to the keloid scars in the same patients (A, B, D), whereas for the back (C), normal skin and keloid scars were obtained from different patients. The images on the right represent enlarged images of the boxed areas indicating the papillary and reticular layers of the dermis in the left-sided images. In the images of keloid scars in (A–C), only the upper parts of the dermal reticular layers are shown. Note that the keloid scars exhibit thickened dermal reticular layers compared to normal skin, with highly dense vasculature in both the papillary and reticular layers. Scale bars: 500 and 100 μm (enlarged images).



upper reticular dermis, to capture the most prominent vascular abnormalities in keloid scars. Furthermore, since keloid scars exhibited thickened dermal reticular layers, we analysed two regions of the reticular layer, Reticular-1 and Reticular-2, corresponding to the areas between 300 and 450 μm and 600 and 750 μm from the top of the papillary layer, respectively, while only the reticular area between 300 and 450 μm from the top of the papillary layer was quantified for normal skin (Figure 4). In the papillary layers that included capillary loops, the vascular density was approximately 1.5 times higher in keloid scars compared to normal skin (Figure 4C). However, the number of vessel branch points relative to the vessel length and the vessel diameter was comparable between keloid scars and normal skin (Figure 4D,E). The reticular layer of normal skin showed less vascularisation, as evidenced by the reduced vascular density compared to the corresponding papillary layer (Figure 4C). In clear contrast, the vascular density and the number of vessel branch points in the upper reticular layer (Reticular-1) were significantly higher in keloid scars than in normal skin, although the vessel diameter was comparable between the two groups. The vascular density in the lower reticular layer (Reticular-2) also tended to be higher in keloid scars compared to the reticular layer of normal skin, although this density was lower than that in Reticular-1. The blood vessels in Reticular-2 were more vertically aligned compared to those in Reticular-1, which might explain the decreased number of branching points in Reticular-2. Collectively, these results indicate that excessive vascularisation is predominantly induced in the papillary and reticular layers of keloid scars, which might contribute to the pathogenesis of keloids.

4 | DISCUSSION

In this study, we successfully visualised the vascular structures in keloids in 3D, using the iDISCO+ tissue clearing technique combined with immunofluorescence staining, enabling analyses of the abnormalities in keloid vasculature in association with its pathogenesis. This approach has the potential to serve as a crucial template for future pathological analyses of abnormal scars.

Our 3D analysis of keloid tissues provided clarification on the long-standing controversy regarding keloid vascularity, which we highlighted in the introduction. Complete evaluation of the vascular structures in keloid scars, imaged using a light sheet fluorescence microscope, revealed spatial heterogeneity in keloid vascularity. In keloid scars, vascular density was higher in superficial regions near the skin surface, while the deeper regions showed reduced vascular density. However, it is noteworthy that the vascular density in the deeper regions of keloids was still higher than that in normal skin. This spatial heterogeneity in vascularisation explains the discrepancies in previous studies,^{16–19} which might have focused on different regions of keloid tissues. By providing a comprehensive 3D view of keloid vasculature, our study reconciles the conflicting reports of both high and low vascular density in keloids found in earlier literature.

The highly vascularised superficial dermis might represent the 'active zone' responsible for the development of keloid lesions.

Previous histological studies have revealed that keloid scars consist of distinct regions at both the cellular and histological levels.^{14,38} Jiao et al. classified keloid tissues into three distinct dermal layers: superficial, mid, and deep dermis, and showed that the superficial dermis exhibited extensive infiltration of lymphocytes and the presence of active fibroblasts, indicating active inflammation in this area. They further showed that the mid dermis contained a prominent number of fibroblasts and compact collagen fibres, while the deep dermis was characterised by low cellularity and thick, disorganised collagen bundles and hyalinised collagen fibres. It is likely that the superficial dermis of keloids corresponds to the highly vascularised superficial dermis, which we characterised in this study, since inflammation and angiogenesis promote each other. Thus, this area likely represents the 'active zone', where inflammatory cells, fibroblasts, and endothelial cells might cooperatively promote angiogenesis, inflammation, and fibrosis, thereby initiating the development of keloid lesions. Indeed, the relationship between vascular structures and fibrosis in keloids has been previously suggested.³⁹ On the other hand, the mid dermis of keloids may correspond to the lower reticular layers, labelled as 'Reticular-2' in Figure 4, where vertically aligned blood vessels are formed. This layer is shown to be populated by fibroblasts and contain few inflammatory cells,³⁸ indicating a lack of inflammation in this area. However, although vascular density decreases in the deeper layers of keloids compared to the superficial layers, it remains significantly higher than in normal skin, emphasising the overall hypervascular nature of keloid tissue (Figure 3). Therefore, the superficial dermis of keloids might transition into the mid dermis as active inflammation and angiogenesis subside, while the active zone simultaneously shifts outward, contributing to the growth of keloid scars. These spatial and temporal changes in vascular structures, angiogenesis, inflammation, and fibrosis within keloids³⁷ offer valuable insights into their pathogenesis and potential therapeutic targets. However, further studies are needed to elucidate the detailed cellular and molecular mechanisms underlying keloid pathogenesis.

Our 3D imaging method for keloid tissues might contribute to a deeper understanding of keloid pathogenesis. In this study, we characterised the comprehensive 3D structure of vasculature in keloid scars. However, this imaging method can also be applied to visualise the 3D localisation and activation status of various other cell types associated with inflammation and fibrosis, providing further insights into keloid lesions. In addition, while the present study provides important insights into the vasculature of keloids, future studies with larger sample sizes and diverse patient demographics could further validate and extend these findings.

In summary, we successfully implemented the iDISCO+ method for clearing keloid scars and, using immunohistochemical staining with CD31 antibodies, accurately determined the 3D structure of vasculature in abnormal scars for the first time. This approach has resolved inconsistencies in previous studies and significantly enhanced our understanding of keloid pathophysiology. Moreover, this method holds promise for future research into the localisation and expression of cells and factors involved in abnormal scar formation. It will also enable researchers to evaluate the impact of current and new

treatments on vascular structures, ultimately aiding in the development of more targeted and effective therapies for keloids.

AUTHOR CONTRIBUTIONS

Teruyuki Dohi, Shigetomo Fukuhara, and Rei Ogawa conceptualised the study. Long Nguyen, Teruyuki Dohi, Haruko Watanabe-Takano, and Shigetomo Fukuhara designed the experiments. Long Nguyen, Teruyuki Dohi, and Rei Ogawa were responsible for sample collection. Long Nguyen and Haruko Watanabe-Takano conducted the tissue experiments. Data analysis was performed by Long Nguyen, Haruko Watanabe-Takano, and Shigetomo Fukuhara. Long Nguyen, Teruyuki Dohi, Haruko Watanabe-Takano, and Shigetomo Fukuhara interpreted the data. Long Nguyen, Teruyuki Dohi, Haruko Watanabe-Takano, Shigetomo Fukuhara, and Rei Ogawa wrote the original draft and revised the manuscript. All authors have read and agreed to the published version of the manuscript.

CONFLICT OF INTEREST STATEMENT

The authors declare no conflicts of interest.

DATA AVAILABILITY STATEMENT

The data that support the findings of this study are available from the corresponding author upon reasonable request.

ORCID

Teruyuki Dohi  <https://orcid.org/0000-0001-7316-8961>

Shigetomo Fukuhara  <https://orcid.org/0000-0003-2777-501X>

Rei Ogawa  <https://orcid.org/0000-0003-3658-555X>

REFERENCES

- Andrews JP, Marttala J, Macarak E, Rosenbloom J, Uitto J. Keloids: the paradigm of skin fibrosis—pathomechanisms and treatment. *Matrix Biol.* 2016;51:37–46.
- Mari W, Alsabri SG, Tabal N, Younes S, Sherif A, Simman R. Novel insights on understanding of keloid scar: article review. *J Am Coll Clin Wound Spec.* 2015;7(1–3):1–7.
- Walsh LA, Wu E, Pontes D, et al. Keloid treatments: an evidence-based systematic review of recent advances. *Syst Rev.* 2023;12(1):42.
- Huang C, Ogawa R. Keloidal pathophysiology: current notions. *Scars Burn Heal.* 2021;7:2059513120980320.
- Zhang M, Chen H, Qian H, Wang C. Characterization of the skin keloid microenvironment. *Cell Commun Signal.* 2023;21(1):207.
- Mogili NS, Krishnaswamy VR, Jayaraman M, Rajaram R, Venkatraman A, Korrapati PS. Altered angiogenic balance in keloids: a key to therapeutic intervention. *Transl Res.* 2012;159(3):182–189.
- Gira AK, Brown LF, Washington CV, Cohen C, Arbisser JL. Keloids demonstrate high-level epidermal expression of vascular endothelial growth factor. *J Am Acad Dermatol.* 2004;50(6):850–853.
- Lei R, Li J, Liu F, et al. HIF-1 α promotes the keloid development through the activation of TGF- β /Smad and TLR4/MyD88/NF- κ B pathways. *Cell Cycle.* 2019;18(23):3239–3250.
- Eura S, Nakao J, Iimura T, et al. Hemodynamics and vascular histology of keloid tissues and anatomy of nearby blood vessels. *Plast Reconstr Surg Glob Open.* 2022;10(6):e4374.
- Fujiwara M, Muragaki Y, Ooshima A. Upregulation of transforming growth factor- β 1 and vascular endothelial growth factor in cultured keloid fibroblasts: relevance to angiogenic activity. *Arch Dermatol Res.* 2005;297(4):161–169.
- Noishiki C, Takagi G, Kubota Y, Ogawa R. Endothelial dysfunction may promote keloid growth. *Wound Repair Regen.* 2017;25(6):976–983.
- Matsumoto NM, Aoki M, Okubo Y, et al. Gene expression profile of isolated dermal vascular endothelial cells in keloids. *Front Cell Dev Biol.* 2020;8:658.
- Matsumoto NM, Peng WX, Aoki M, et al. Histological analysis of hyalinised keloidal collagen formation in earlobe keloids over time: collagen hyalinisation starts in the perivascular area. *Int Wound J.* 2017;14(6):1088–1093.
- Bux S, Madaree A. Keloids show regional distribution of proliferative and degenerate connective tissue elements. *Cells Tissues Organs.* 2010;191(3):213–234.
- Shim J, Oh SJ, Yeo E, et al. Integrated analysis of single-cell and spatial transcriptomics in keloids: highlights on fibrovascular interactions in keloid pathogenesis. *J Invest Dermatol.* 2022;142(8):2128–2139.e11.
- Amadeu T, Braune A, Mandarim-de-Lacerda C, Porto LC, Desmouliere A, Costa A. Vascularization pattern in hypertrophic scars and keloids: a stereological analysis. *Pathol Res Pract.* 2003;199(7):469–473.
- Kurokawa N, Ueda K, Tsuji M. Study of microvascular structure in keloid and hypertrophic scars: density of microvessels and the efficacy of three-dimensional vascular imaging. *J Plast Surg Hand Surg.* 2010;44(6):272–277.
- Liang ZY, Wang YW, Hao Y, et al. Histopathologic study of keloid vascular structures shows the vascular origin pattern of keloid subepidermal vascular network flaps. *Am J Transl Res.* 2023;15(3):1889–1896.
- Ueda K, Yasuda Y, Furuya E, Oba S. Inadequate blood supply persists in keloids. *Scand J Plast Reconstr Surg Hand Surg.* 2004;38(5):267–271.
- Seo J, Choe M, Kim SY. Clearing and labeling techniques for large-scale biological tissues. *Mol Cells.* 2016;39(6):439–446.
- Dotdt HU, Leischner U, Schierloh A, et al. Ultramicroscopy: three-dimensional visualization of neuronal networks in the whole mouse brain. *Nat Methods.* 2007;4(4):331–336.
- Susaki EA, Ueda HR. Whole-body and whole-organ clearing and imaging techniques with single-cell resolution: toward organism-level systems biology in mammals. *Cell Chem Biol.* 2016;23(1):137–157.
- Susaki EA, Tainaka K, Perrin D, et al. Whole-brain imaging with single-cell resolution using chemical cocktails and computational analysis. *Cell.* 2014;157(3):726–739.
- Touloumes GJ, Ardonna HAM, Casalino EK, et al. Mapping 2D- and 3D-distributions of metal/metal oxide nanoparticles within cleared human ex vivo skin tissues. *NanoImpact.* 2020;17:17.
- Ueda M, Saito S, Murata T, et al. Combined multiphoton imaging and biaxial tissue extension for quantitative analysis of geometric fiber organization in human reticular dermis. *Sci Rep.* 2019;9(1):10644.
- Tan Y, Ng WJ, Lee SZX, et al. 3-Dimensional optical clearing and imaging of pruritic atopic dermatitis and psoriasis skin reveals down-regulation of epidermal innervation. *J Invest Dermatol.* 2019;139(5):1201–1204.
- Tan Y, Chiam CPL, Zhang Y, Tey HL, Ng LG. Research techniques made simple: optical clearing and three-dimensional volumetric imaging of skin biopsies. *J Invest Dermatol.* 2020;140(7):1305–1314.e1.
- Watanabe-Takano H, Fukumoto M, Fukuhara S, Mochizuki N. Protocol for whole-mount X-gal staining combined with tissue clearing in embryo and adult mouse using CUBIC. *STAR Protoc.* 2022;3(1):101127.
- Tainaka K, Kubota SI, Suyama TQ, et al. Whole-body imaging with single-cell resolution by tissue decolorization. *Cell.* 2014;159(4):911–924.
- Renier N, Wu Z, Simon DJ, Yang J, Ariel P, Tessier-Lavigne M. iDISCO: a simple, rapid method to immunolabel large tissue samples for volume imaging. *Cell.* 2014;159(4):896–910.



31. Otomo K, Omura T, Nozawa Y, et al. descSPIM: an affordable and easy-to-build light-sheet microscope optimized for tissue clearing techniques. *Nat Commun*. 2024;15(1):4941.
32. Elfarnawany MHE-K. *Signal Processing Methods for Quantitative Power Doppler Microvascular Angiography*. The University of Western Ontario (Canada); 2015.
33. Arganda-Carreras I, Fernandez-Gonzalez R, Munoz-Barrutia A, Ortiz-De-Solorzano C. 3D Reconstruction of histological sections: application to mammary gland tissue. *Microsc Res Tech*. 2010;73(11):1019-1029.
34. Li X, Mao Z, Yang L, Sun K. Co-staining blood vessels and nerve fibers in adipose tissue. *J Vis Exp*. 2019;144. doi:[10.3791/59266](https://doi.org/10.3791/59266)
35. Braverman IM. The cutaneous microcirculation. *J Invest Dermatol Symp Proc*. 2000;5(1):3-9.
36. Ricci V, Ricci C, Cocco G, et al. From histology to sonography in skin and superficial tissue disorders: EURO-MUSCULUS/USPRM* approach. *Pathol Res Pract*. 2022;237:154003.
37. Jumper N, Paus R, Bayat A. Functional histopathology of keloid disease. *Histol Histopathol*. 2015;30(9):1033-1057.
38. Jiao H, Zhang T, Fan J, Xiao R. The superficial dermis may initiate keloid formation: histological analysis of the keloid dermis at different depths. *Front Physiol*. 2017;8:885.
39. Ogawa R, Akaishi S. Endothelial dysfunction may play a key role in keloid and hypertrophic scar pathogenesis—keloids and hypertrophic scars may be vascular disorders. *Med Hypotheses*. 2016; 96:51-60.

SUPPORTING INFORMATION

Additional supporting information can be found online in the Supporting Information section at the end of this article.

How to cite this article: Nguyen L, Dohi T, Watanabe-Takano H, Fukuhara S, Ogawa R. Comprehensive analysis of keloid vasculature by tissue clearing and 3D imaging. *Wound Rep Reg*. 2025;33(2):e70015. doi:[10.1111/wrr.70015](https://doi.org/10.1111/wrr.70015)